



Microstructure characterization and mechanical properties of the continuous-drive axial friction welded aluminum/stainless steel joint

Yong Liu^{1,2} · Haiyan Zhao¹ · Yun Peng² · Xiaofei Ma³

Received: 11 April 2019 / Accepted: 1 August 2019 / Published online: 22 August 2019
© Springer-Verlag London Ltd., part of Springer Nature 2019

Abstract

Aluminum alloy and stainless steel were joined by a continuous-drive axial friction welding machine in this study. The effects of welding parameters on the morphology, microstructure, microhardness, tensile strength, and fracture surface of dissimilar joints were analyzed. The distribution, thickness, and composition of intermetallic compound (IMC) were also discussed. Results showed that the formation of flash only was on the aluminum side because 6061 Al underwent extensive deformation during welding. Al and Fe elements diffused at the bonding interface and formed the IMC layer. The IMC thickness near the 1/2 radius was the smallest, and the thinnest at the center region. With the increase of friction pressure, the tensile strength of joint first increased and then decreased. When forge pressure was below 220 MPa, joint strength was approximately linearly related to the forge pressure. Edge regions of joints had achieved metallurgical bonding. The central region was the weak joining, and the fracture surface contained some cracks, IMCs, and a small amount of dimples.

Keywords Friction welding · The dissimilar welded joint · Microstructure · Tensile strength · Impact strength

1 Introduction

The joining of dissimilar metals has wide industrial applications, particularly in the aerospace and nuclear industries. Development of dissimilar metal weldments represents major challenge in modern manufacturing process, and this is very crucial in developing sound dissimilar weldments in the future [1, 2]. Nevertheless, it is sufficiently difficult to attain good-quality dissimilar joints of these two kinds of alloys because of their physical, mechanical, and thermal properties [3–5].

Hybrid structures of aluminum alloy and steel have attracted much attention for combining fine mechanical properties of steel with low density and good corrosion resistance of aluminum alloy [6, 7]. Research conducted on welding of aluminum alloy to steel ranges from fusion to solid-state welding processes [8, 9]. Friction welding is a solid-state joining method and has extensively been used because of the advantages such as high material saving and low production time [10, 11]. This method is very useful for the joining of dissimilar combination, and welding process is easily automated [12]. Continuous-drive friction welding is the most common form in friction welding due to the high energy efficiency, narrower heat-affected zone (HAZ), and low welding cost [13, 14]. Friction time, friction pressure, forge pressure, and rotation speed are the most important parameters in friction welding. These process parameters directly affect welding quality [15].

Although feasibility of friction welded Al/steel joints has already been confirmed, the challenge of dissimilar metal friction welding is associated not only with their individual properties, but also with the reactions taking place at the interface. These reactions will lead to the occurrence of brittle intermetallic phases or other undesired components. The low solubility of Fe in Al results in the formation of thick and brittle Al-

✉ Yong Liu
liuyong1350130711@126.com

✉ Haiyan Zhao
hyzhao@tsinghua.edu.cn

✉ Yun Peng
pengyun@cisri.com.cn

¹ School of Materials Science and Engineering, Tsinghua University, Beijing 100084, China

² China Iron & Steel Research Institute Group, Beijing 100081, China

³ School of Materials Science and Engineering, Shandong University, Jinan 250061, China

rich intermetallic compound (IMC) due to high heat input, which will lead to the degradation of mechanical property [16].

Several studies about the joining of aluminum alloys to steels by friction welding have been reported [12, 17–19]. Lee et al. studied the effect of friction welding parameters on mechanical and metallurgical properties of Al/Fe joint [20]. In order to obtain the high joint efficiency and bend ductility, Kimura et al. found that the aluminum/stainless steel friction welded joint should be made with such a high forge pressure as 150 MPa, and with the opportune friction time that the temperature on the weld interface reached to about 573 K or higher [21]. Kobayashi et al. have investigated the possibility of joining conventional steel and aluminum alloy using friction welding, and found that the good strength of the aluminum/steel welded joint could be obtained. The IMC was not found at the cross-sectional interface, but observed at the fracture interface after tensile test [22]. Fukumoto et al. found that sufficient heat to obtain a sound joint could not be generated with a shorter friction time, but the longer friction time caused the excess formation of an intermetallic layer [23].

The thickness distribution and formation of IMC, the analysis of heat-affected zone softening, and their relationships with mechanical properties need to be further research. In this study, the joining capability of 6061 aluminum alloy and 304 stainless steel was studied by the continuous-drive friction welding. After welding, tensile and hardness experiments of joints were carried out. Microstructural features and fracture surface were investigated by the optical microscope and scanning electron microscopy (SEM). Energy-dispersive spectroscopy (EDS) and XRD analysis were carried out for chemical composition and phase investigation on welding and fracture surface.

2 Experimental procedure

2.1 Base metals

Base metals were 6061-T6 aluminum alloy (6061 Al) and 304 stainless steel (304 SS) in 15-mm-diameter rods. Chemical compositions of base metals are listed in Table 1.

Table 1 Chemical compositions of 6061-T6 aluminum alloy and 304 stainless steel (wt%)

Metal	Fe	Mg	Si	Mn	Cu	Cr	Zn	Ni	Al
6061-T6	0.73	1.02	0.69	0.13	0.20	0.10	0.28	0.05	Balance
304 SS	71.7	–	0.62	1.44	0.30	17.15	1.10	8.15	0.01

2.2 Friction welding process

A continuous-drive friction welding machine was used to join base metals. The welding process includes four stages: initial friction, stable friction, braking, and forging. During welding process, the main motor kept 6061 aluminum alloy rods to maintain a constant rotation speed, and 304 SS rods moved slowly and was close to the rotating 6061 Al rod under the friction pressure. The friction heat was generated when two rods connected, and then reached the stable friction stage. After the friction, the forging pressure was applied to stop the rotation, and two base metals realized welding. The spindle speed of 2200 rpm and upsetting time of 8 s were the fixed process parameters. The adjustable process parameters included friction pressure (P_1), friction time (t), and forge pressure (P_2). It should be noted that friction time was the sum of stable friction time and braking time in this experiment. Because the rotation of rod was not instantly stopping when joints were made by a continuous-drive friction welding machine, the joint had the deformation at the braking during rotation stop [24].

The aluminum/steel dissimilar material continuous-drive friction welding test is shown in Fig. 1. The butt joint is used. The 6061 Al is the rotating axis side, and the 304 SS is the fixing axis side. To collect the steel-side temperature of joint, a blind hole having a diameter of 1.5 mm was vertically machined through a drill press at a distance of 0.5 mm from the end face of the moving side steel-side bar. The thermocouple wire was passed through the ceramic tube and inserted into the blind hole. The high-temperature glue was used to fix the contact part. The welding temperature is collected as shown in Fig. 1.

2.3 Characterization

The microstructural observation of specimen was cut perpendicular to the welding interface by the electrical discharge

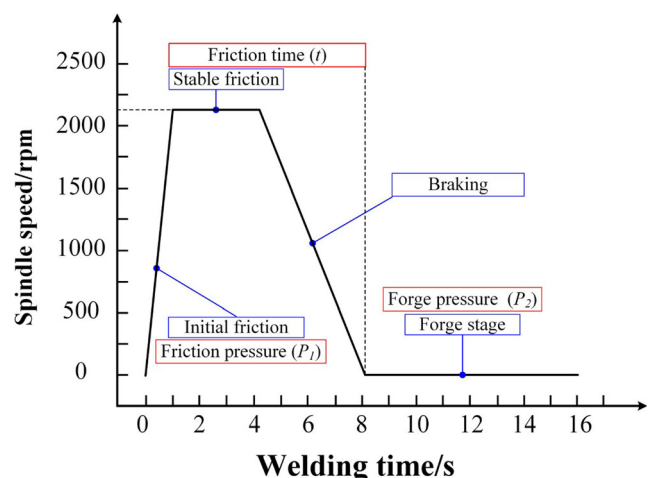


Fig. 1 The process profile of continuous-drive friction welding

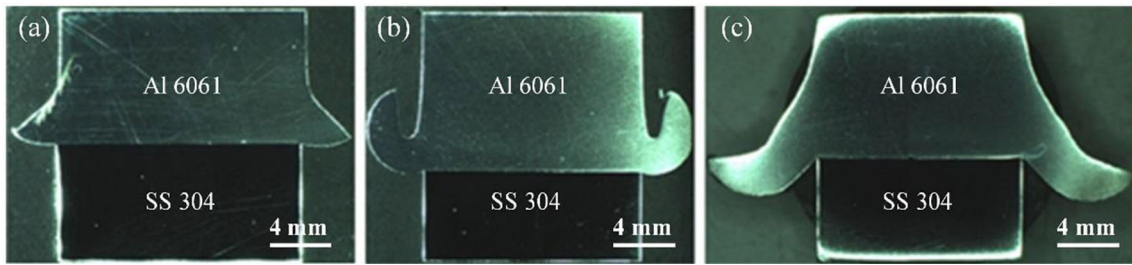


Fig. 2 Influence of process parameters on the joint morphology: (a) $P_1 = 40$ MPa, $P_2 = 120$ MPa, $t = 4$ s; (b) $P_1 = 40$ MPa, $P_2 = 220$ MPa, $t = 4$ s; (c) $P_1 = 40$ MPa, $P_2 = 220$ MPa, $t = 6$ s

machine. The 304 SS side was etched by the solution (2.5 mL HNO_3 and 97.5 mL ethanol), and the 6061 Al side was etched by Keller’s reagent (1.0 mL HF, 1.5 mL HCl, 2.5 mL HNO_3 , and 95 mL H_2O). The microstructure was observed by optical microscopy (OM) and SEM machine. The Vickers hardness distribution of joints was measured using a microhardness tester. The indentation load was 200 g and dwell time was 10 s. The interval between the adjacent indentations was 0.5 mm.

Three tensile specimens were prepared based on GB/T228.1-2010, and the ultimate tensile load of welded joint was measured by the universal material testing machine. Tensile tests were performed at ambient temperature under a crosshead speed of 0.5 mm/min. The tensile strengths of the welded joints were calculated by dividing the ultimate tensile load by an area of 15 mm diameter. The fracture surface of the tensile specimens was characterized by SEM and XRD methods.

3 Results and discussion

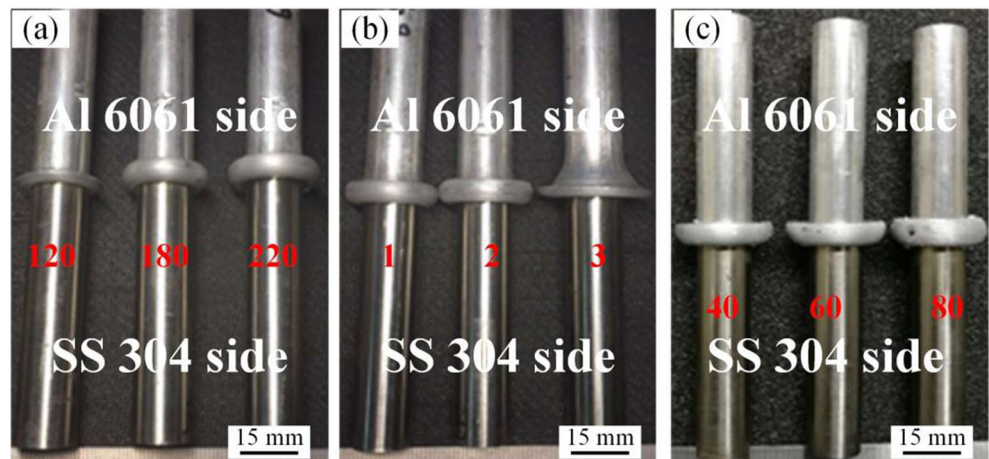
3.1 Morphology of the welded joint

Figure 2 shows the morphology of joint under different process parameters. A welding flash was formed when

metal was being pushed along the direction of the weld edges. The 304 SS has a lower thermal conductivity and greater hardness at high temperatures compared with 6061 Al. Thus, 304 SS did not undergo extensive deformation while 6061 Al underwent extensive deformation during welding. The formation of flash was only on the aluminum side, and the flash distributed symmetrically on the aluminum side and surrounded gradually the joining interface. As forge pressure increased, much plastically deformation was extruded, which resulted to the growth of flash, as shown in Fig. 2b. In particular, due to the excessive friction time, a large amount of deformation metal was generated, and a wrap-like flash was formed and the flash edge morphology was also significantly different from the other welded joints, as shown in Fig. 2c. The macrostructure of the friction welded joint showed that the friction welded joint had the clear interface and no obvious voids and cracks.

The process parameters not only determined the morphology, but also influenced the axial shortening, as shown in Fig. 3. Figure 4 shows the axial shortening of joints under different process parameters. The axial shortening of joints increased with the forge pressure, friction time, and pressure. The friction time had the largest impact on the axial shortening (Fig. 4b). The aluminum side of joint formed the uniform flash under different process parameters.

Fig. 3 Influence of process parameters on joint morphology: (a) forge pressure ($P_1 = 40$ MPa; $t = 4$ s); (b) friction time ($P_1 = 40$ MPa; $P_2 = 220$ MPa); (c) friction pressure ($t = 4$ s; $P_2 = 220$ MPa)



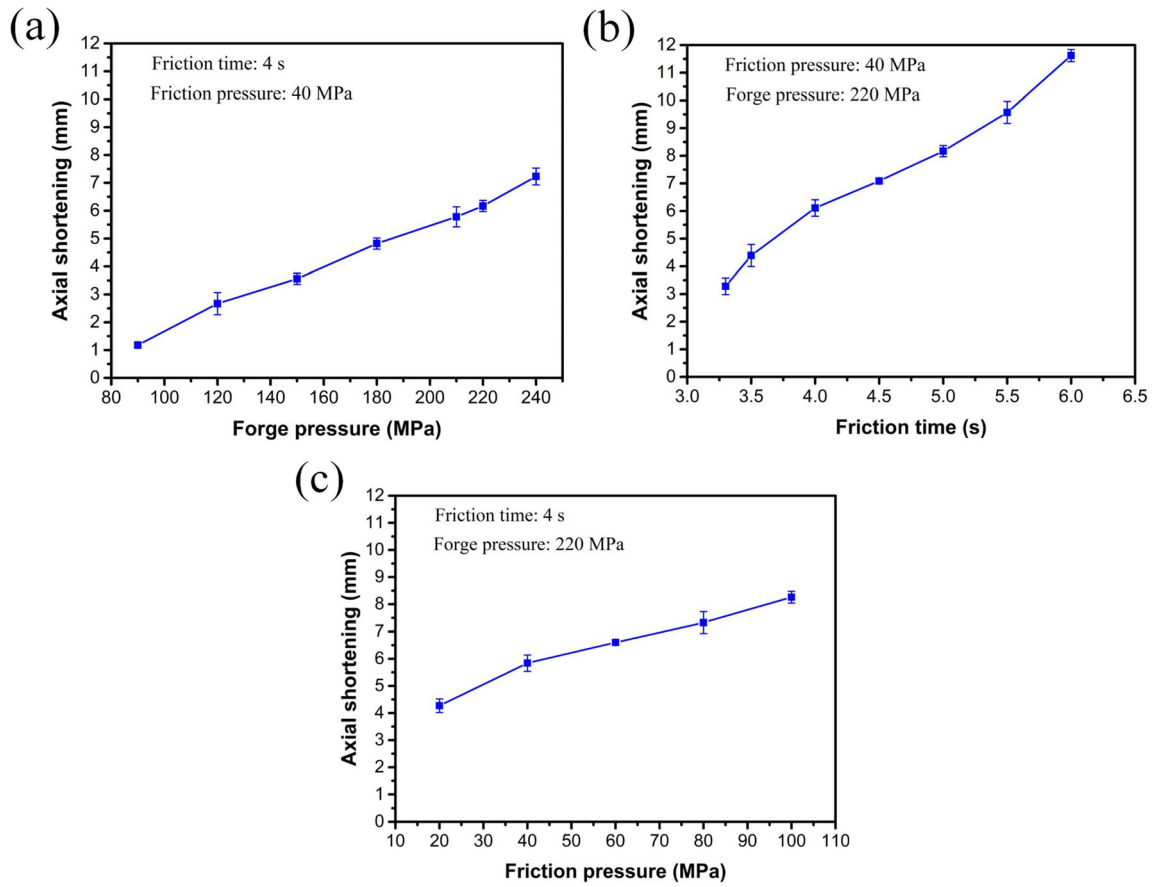


Fig. 4 Influence of process parameters on the axial shortening: (a) forge pressure ($P_1 = 40$ MPa; $t = 4$ s); (b) friction time ($P_1 = 40$ MPa; $P_2 = 220$ MPa); (c) friction pressure ($t = 4$ s; $P_2 = 220$ MPa)

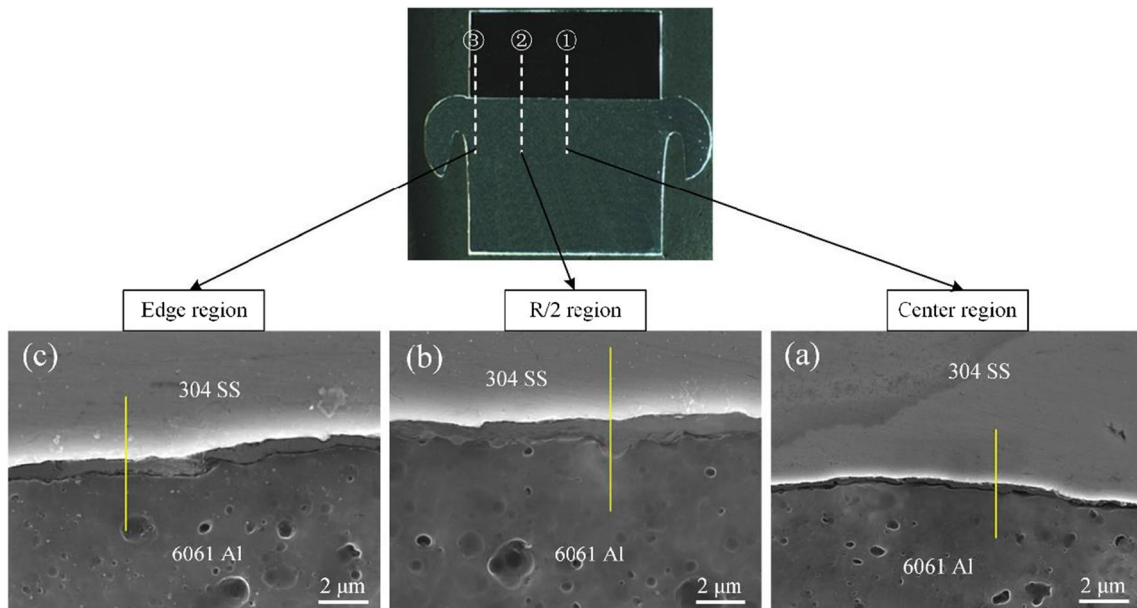


Fig. 5 The SEM images of bonding interface and the EDS line scanning results at different measured positions ($P_1 = 40$ MPa, $t = 4$ s, $P_2 = 220$ MPa): (a) the edge of the welded joint; (b) the R/2 position; (c) the center of welded joint

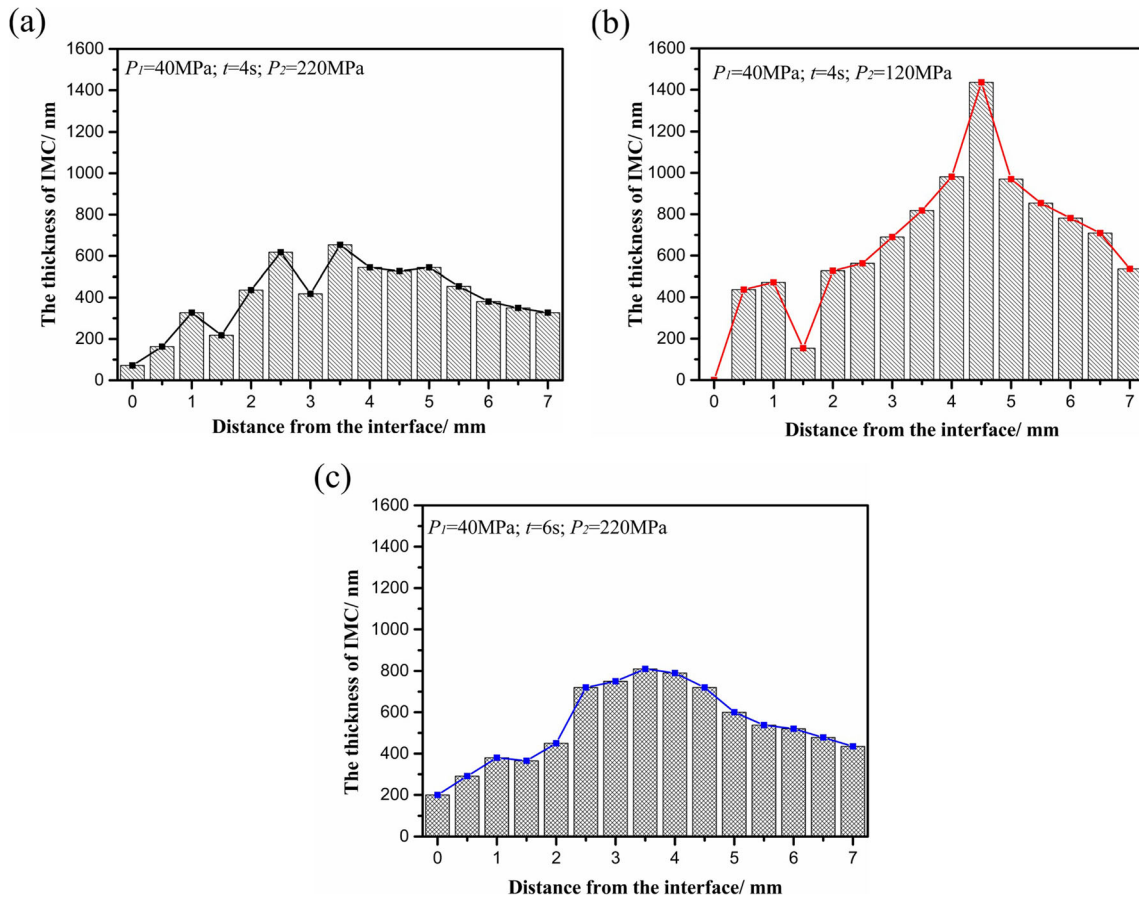


Fig. 6 Distribution of IMC thickness at the interface of joint: (a) $P_1 = 40\text{ MPa}$, $P_2 = 220\text{ MPa}$, $t = 4\text{ s}$; (b) $P_1 = 40\text{ MPa}$, $P_2 = 120\text{ MPa}$, $t = 4\text{ s}$; (c) $P_1 = 40\text{ MPa}$, $P_2 = 220\text{ MPa}$, $t = 6\text{ s}$

3.2 Microstructure of the welded joint

Al and Fe elements generated diffusion at the bonding interface and formed the IMC layer. The IMC layer was relatively flat on the 304 SS side, while uneven on the 6061 Al side. Because atom diffusion rate in the compound was not the same due to the different atomic radii of Al and Fe, the self-diffusion coefficient of Al atom was relatively larger and diffused faster than Fe atom [25]. The microstructure of joint at different regions is shown in Fig. 5.

The interfacial reaction and composition of Al/Fe dissimilar joints were complicated. The main IMC formed in the reaction layer were Al_5Fe_2 and $\text{Al}_{13}\text{Fe}_4$ phases with local silicon enrichment. The formation process of IMC was as follows [26]: iron dissolved into the aluminum melt when the iron concentration reached to its maximum solubility, and the dissolved iron crystallized to form $\text{Al}_{13}\text{Fe}_4$ during solidification. $\text{Al}_{13}\text{Fe}_4$ phase initially formed at the liquid interface and then decomposed to form Al_5Fe_2 in the layer of $\text{Al}_{13}\text{Fe}_4/\text{Fe}$. Huang et al. [27] found that fine steel fragments in IMC layer dissolve in the Al and

Fig. 7 Effect of process parameters on microhardness (R/2 measured position, friction pressure 40 MPa): (a) friction time; (b) forge pressure

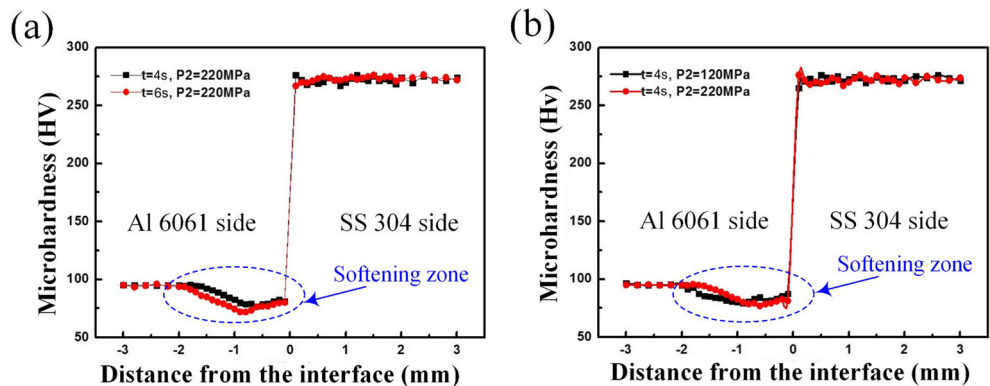
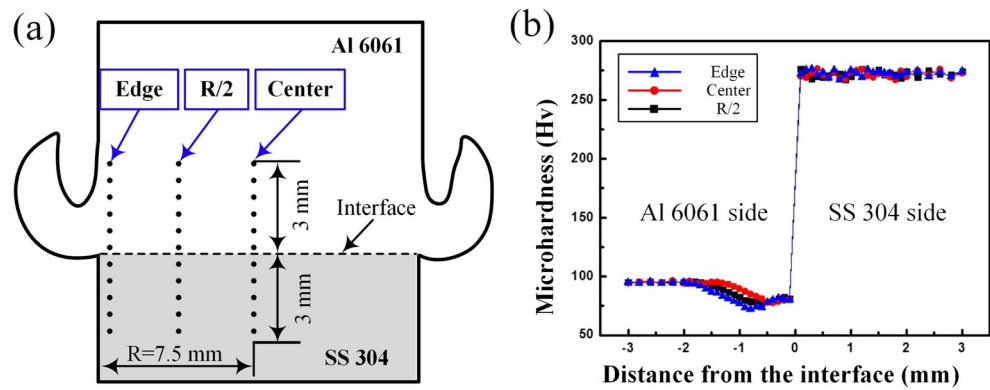


Fig. 8 Microhardness of different measured positions of the welded joints ($P_1 = 40$ MPa, $P_2 = 220$ MPa, $t = 4$ s): (a) measured position; (b) microhardness distribution



then lead to the nucleation of nano $\text{Al}_{13}\text{Fe}_4$ crystals due to severe shear force and Fe outward diffusion. However, Camille et al. [28] found that the intermetallic reaction layer was formed at the interface with the steel sheet due to the reactivity between the molten Al and the solid steel, and the IMC layer contained Al_3Fe and Al_5Fe_2 . Al_3Fe layer had local silicon enrichment according to compositional information, and its structure was polycrystalline, not amorphous [29].

In order to analyze the formation of IMC layer and the degree of metallurgical bonding, the interfacial microstructure of joints under different process parameters and the thickness of the IMC layer at different positions were measured according to the SEM images, as shown in Fig. 6. The results showed that the thickness of IMC layer was not uniform. The IMC thickness near the 1/2 radius was the thickest, and the thinnest at the center

region. The reason should be that the edge region experienced the stronger thermomechanical effect and more complete metallurgical reaction due to the higher linear velocity than the center region of joint.

The distribution of IMC layer at the bonding interface and its formation behavior changed with the positions. By comparing the IMC thickness under different forge pressures, the high-temperature shaping metal was easily tended to flow outward and squeezed into the flash when forge pressure increased, which finally reduced the IMC thickness, as shown in Fig. 6a and b. When the friction time increased, the metal involved in plastic deformation increased, and the diffusion of Al and Fe atoms was more sufficient to promote the metallurgical reaction. Finally, the thickness of IMC layer became thick, as shown in Fig. 6c.

Fig. 9 Influence of process parameters on the tensile strength: (a) friction pressure ($t = 4$ s; $P_2 = 220$ MPa); (b) forge pressure ($P_1 = 40$ MPa; $t = 4$ s); (c) friction time ($P_1 = 40$ MPa; $P_2 = 220$ MPa)

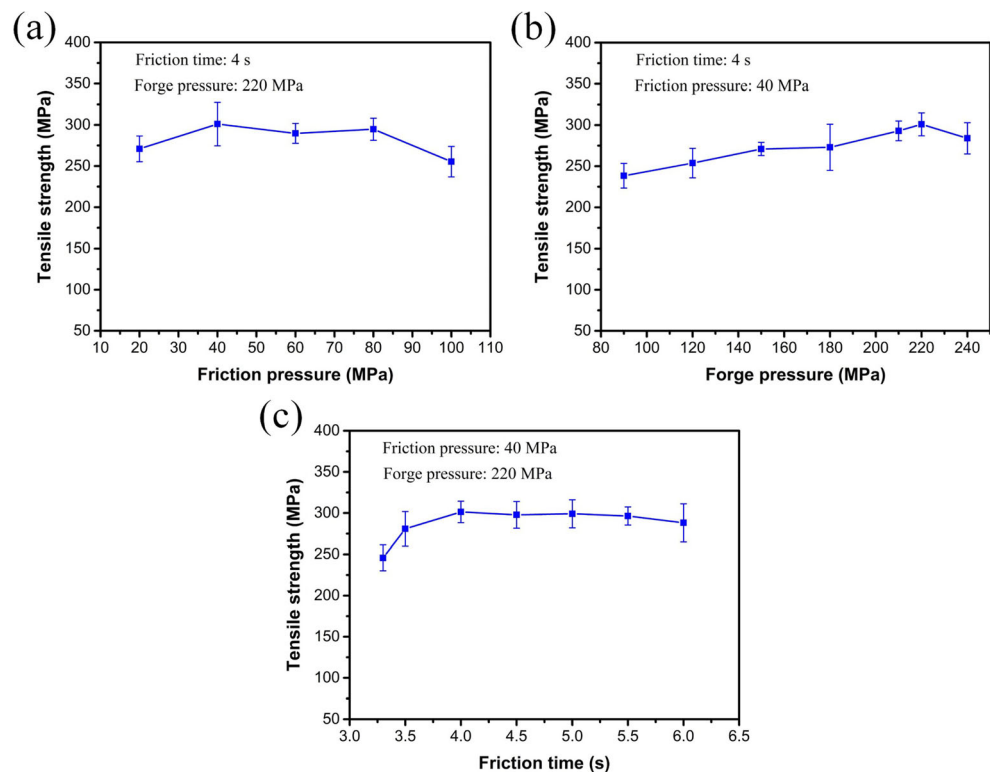
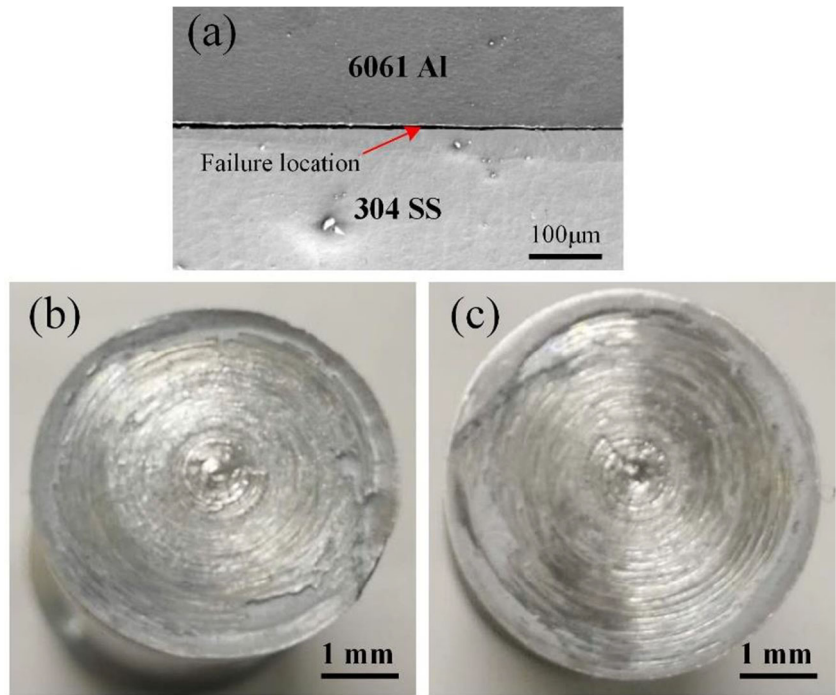


Fig. 10 Fracture surface of the welded joint after tensile testing ($P_1 = 40$ MPa; $t = 4$ s; $P_2 = 220$ MPa): (a) the failure location; (b) 6061 Al side; (c) 304 SS side



3.3 Microhardness of the welded joint

Figure 7 shows the effects of friction time and forge pressure on the microhardness. Because the aluminum base metal underwent both the welding thermal cycle and the axial pressure during the friction process, some strengthening phase would dissolve into the aluminum matrix at high temperature, which resulted to the formation of softening zone. With the extent of friction time, the width of softening zone increased relatively due to the formation of large plastic deformation (Fig. 7a). Because more plastic deformation layer was squeezed into the flash edge, the width of softening zone became narrow with the increase of forge pressure, as shown in Fig. 7b. Post-weld heat treatment was able to prevent loss of joint strength through ensuring softened zone hardness recovery. However, this technique does not apply to non-heat-treatable alloys [30].

For the dissimilar metal welded joint, their physical and chemical properties were different. The hardness of 304 SS was about 3 times that of the 6061 Al. The 304 SS steel hardly underwent plastic deformation, and its microhardness almost

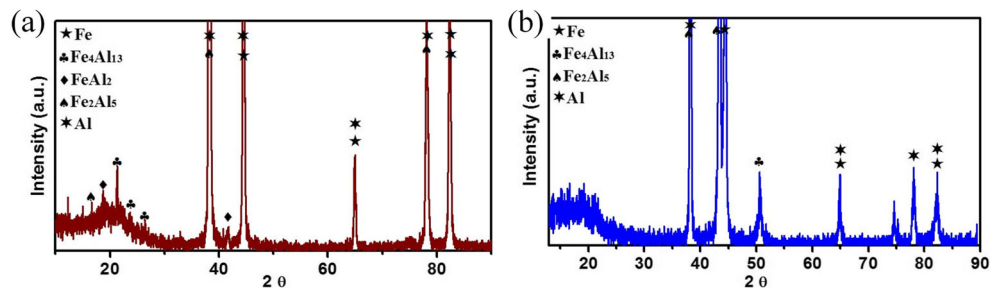
did not influence, while the microhardness of 6061 Al base metal was slightly changed at different measured positions, as shown in Fig. 8. The reason should be that the central region of joint experienced less plastic deformation and the width of the softened region was narrow.

3.4 Tensile strength of the welded joint

Figure 9a shows the correlation between friction pressure and tensile strength of joint. With the increase of friction pressure, the tensile strength of joint first increased and then decreased. When the friction pressure was 40 MPa, the joint average strength could reach the maximum value of 304 MPa. The high friction pressure could break the oxide film on the surface of the aluminum base material, which the metallurgical reactions occurred sufficiently. However, the excessive frictional pressure would generate much heat input, and cause severe softening of the heat-affected zone on the aluminum alloy side and decrease the tensile strength of joint.

Figure 9b shows the influence of forge pressure on the tensile strength of welded joints. When forge pressure was

Fig. 11 The XRD patterns of the fracture surface of the welded joint: (a) 6061Al side; (b) 304 SS side



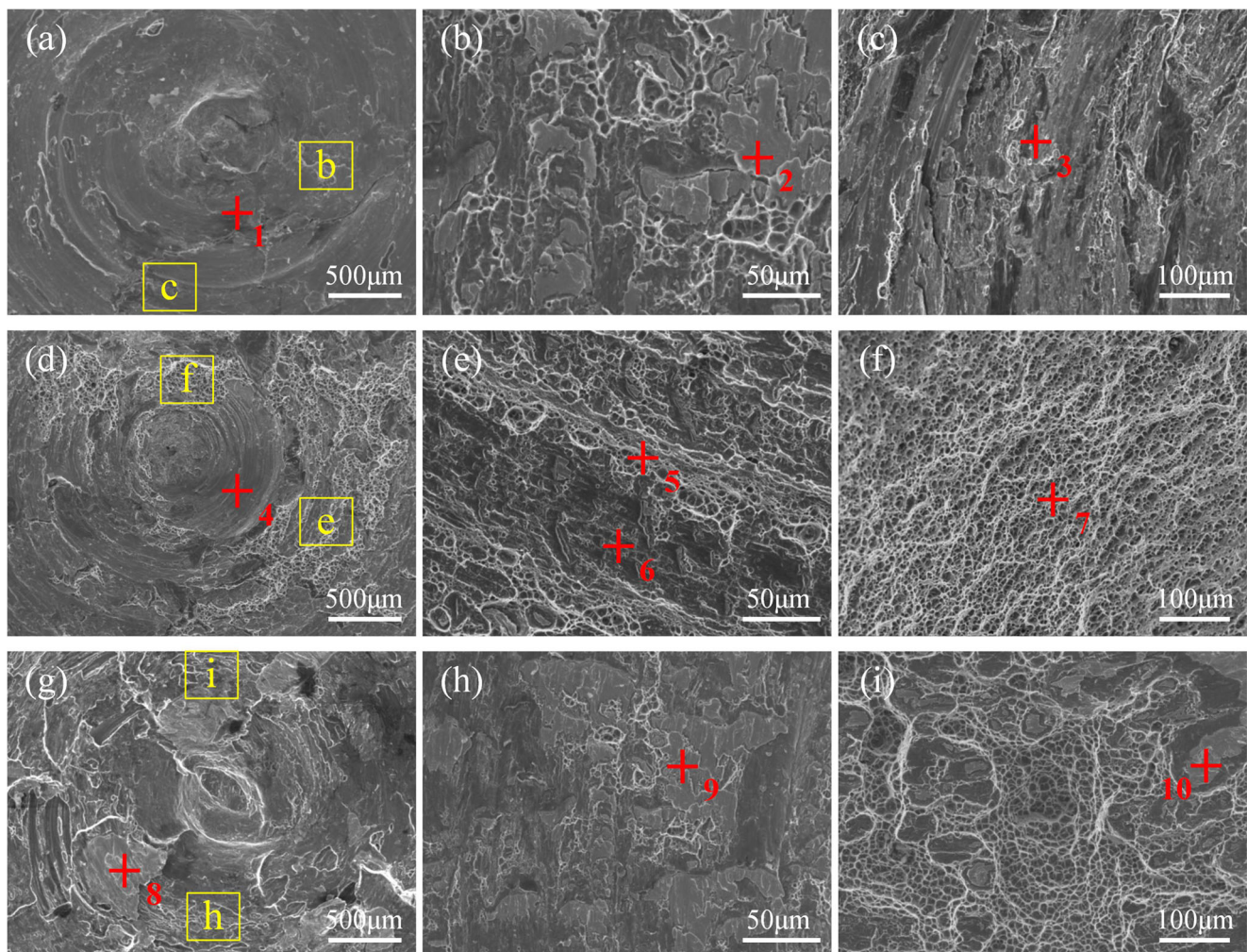


Fig. 12 SEM images of fracture surface of the welded joint with different process parameters: (a–c) $P_1 = 40$ MPa, $P_2 = 120$ MPa, $t = 4$ s; (d–f) $P_1 = 40$ MPa, $P_2 = 220$ MPa, $t = 4$ s; (g–i) $P_1 = 40$ MPa, $P_2 = 220$ MPa, $t = 6$ s

below 220 MPa, the strength of joint was approximately linearly related to the forge pressure. Since the thickness of IMC layer was greatly affected by the forge pressure, the influence of forge pressure on the tensile strength of the welded joint

Table 2 The composition of position in Fig. 12 (at.%)

Point	Al	Fe
1	1.19	98.81
2	71.78	28.22
3	9.24	90.76
4	4.83	95.17
5	90.22	9.78
6	73.25	26.75
7	93.16	6.84
8	74.37	25.63
9	67.75	32.25
10	70.53	29.47

was more significant than that of the frictional pressure. Figure 9c shows the correlation between friction time and tensile strength of the welded joint. The tensile strength increased gradually with the increase of friction time. While the friction time increased, the width of softening zone on the aluminum side increased and the joint strength decreased.

3.5 Fracture surface of the welded joint after tensile test

Although high-quality welded joints can be obtained by optimizing friction welding parameters, all friction welded specimens break at the friction interface during tensile test, as shown in Fig. 10. The central area of fracture surface on the steel side was smooth and had almost no sign of ductile fracture. Some trace of IMCs could be observed on the fracture surface, which would affect the mechanical properties of friction welded joint. Apparent tear was observed in the edge of the aluminum side fracture.

In order to determine the phase composition of fracture surface, fracture surface was measured by XRD, as showed in Fig. 11. XRD results showed that the obvious diffraction peaks of Al, Fe₂Al₅, Fe, and Fe₄Al₁₃ phases were detected on both the fracture surfaces. The presence of Fe₂Al₅ IMCs indicated joint had formed the metallurgical frictional interface. However, too much brittle and hard phase would also reduce the tensile strength of joint.

Figure 12 shows the SEM images of the steel-side fracture surface, and Table 2 shows the EDS elemental analysis results. In the center of joint, there were a certain number of cracks and annular tear marks (Fig. 12a). The chemical composition of point 1 was 98.81% Fe and 1.19% Al, indicating that this region was mainly steel matrix and almost not metallurgical bonding under this parameter. The fracture morphology of the 1/2 radius region consisted of a small number of dimples and lamellar structures, and the composition of point 2 was 28.22% Fe and 71.78% Al. In the edge region of joint (Fig. 12c), the fracture surface was mainly composed of Fe, indicating that the edge region did not form the metallurgical bonding. Because the thermal conductivity of base metals varied greatly, a large amount of heat was transferred through the Al side during welding. The energy used to form joints on the friction welding interface was relatively small, resulting in the interface does not fully form metallurgical bonding under these process parameters. Metallurgical bonding required sufficient heat conditions for the full diffusion of metal atoms.

Figure 12d–f show the fracture SEM images of joint under the process parameter ($P_1 = 40$ MPa, $P_2 = 220$ MPa, $t = 4$ s). Compared with the forge pressure of 120 MPa, the central region was tightly bonded, and some dimples were attached on the steel substrate. The 1/2 radius region was composed of a series of dimples and lamellar structure. EDS results show that there were many Fe/Al intermetallic compounds in the region. The edge region had a large number of aluminum matrix tear dimples.

When the process parameters were $P_1 = 40$ MPa, $P_2 = 220$ MPa, $t = 6$ s, the steel-side fracture surfaces of the welded joint are shown in Fig. 12h and i. There were many interlaminar IMCs in the joint. EDS results showed that the chemical composition at these regions was Fe₂Al₅, indicating that joint achieved metallurgical bonding. However, due to the long friction time, many brittle hard phases were formed and joint fracture was related to the existence of brittle phase at the friction interface.

Based on the above results, joints had achieved metallurgical bonding due to thermal coupling. The majority of thermal energy was caused by the relative movement and material plastic deformation between base metals. However, the energy density was not uniform, and roughly proportional to the radial distance [31]. For welded joints of dissimilar aluminum alloys and steels, one common feature is the formation of IMC at the interface between Al and steel alloys and one of the most

important thing is how to control the amount of reactant [32, 33]. The thickness of IMC layer increases with the increase of heat and it is also a fundamental prerequisite to obtain welded joints with good performance [34, 35].

4 Conclusions

- (1) 304 SS did not undergo extensive deformation while 6061 Al underwent extensive deformation during welding. The flash was only on the aluminum side, and the flash distributed symmetrically.
- (2) Al and Fe elements diffused at the bonding interface and formed the IMC layer. The IMC thickness near the 1/2 radius was the smallest, and the thinnest at the center region. The distribution of IMC layer at the bonding interface and its formation behavior changed with the positions.
- (3) With the extent of friction time, the width of softening zone increased relatively due to the formation of large plastic deformation. The width of softening zone became narrow with the increase of forge pressure. As the increase of friction pressure, tensile strength of joint first increased and then decreased. When forge pressure was below 220 MPa, joint strength was approximately linearly related to the forge pressure.
- (4) Edge regions of joints had achieved metallurgical bonding. The central region was the weak joining, and the fracture surface contained some cracks, IMCs, and a small amount of dimples.

References

1. Reddy MG, Rao SA, Mohandas T (2008) Role of electroplated interlayer in continuous drive friction welding of AA6061 to AISI 304 dissimilar metals. *Sci Technol Weld Join* 13(7):619–628
2. Karakizis PN, Pantelis DI, Dragatogiannis DA, Bougiouri VD, Charitidis CA (2019) Study of friction stir butt welding between thin plates of AA5754 and mild steel for automotive applications. *Int J Adv Manuf Technol* 102(9):3065–3076
3. Huang Y, Huang T, Wan L, Meng X, Zhou L (2019) Material flow and mechanical properties of aluminum-to-steel self-riveting friction stir lap joints. *J Mater Process Technol* 263:129–137
4. Bhamji I, Preuss M, Threadgill PL, Addison AC (2011) Solid state joining of metals by linear friction welding: a literature review. *Mater Sci Technol* 27(1):2–12
5. Derazkola HA, Khodabakhshi F (2019) Underwater submerged dissimilar friction-stir welding of AA5083 aluminum alloy and A441 AISI steel. *Int J Adv Manuf Technol* 102(9):4383–4395
6. Wan L, Huang Y (2018) Friction welding of AA6061 to AISI 316L steel: characteristic analysis and novel design equipment. *Int J Adv Manuf Technol* 95(9):4117–4128
7. Wang T, Sidhar H, Mishra RS, Hovanski Y, Upadhyay P, Carlson B (2018) Friction stir scribe welding technique for dissimilar joining of aluminium and galvanised steel. *Sci Technol Weld Join* 23(3): 249–255

8. Ogawa D, Kakiuchi T, Hashiba K, Uematsu Y (2019) Residual stress measurement of Al/steel dissimilar friction stir weld. *Sci Technol Weld Join*:1–10
9. Abioye TE, Mustar N, Zuhailawati H, Suhaina I (2019) Prediction of the tensile strength of aluminium alloy 5052-H32 fibre laser weldments using regression analysis. *Int J Adv Manuf Technol* 102(5):1951–1962
10. Sahin M (2007) Evaluation of the joint-interface properties of austenitic-stainless steels (AISI 304) joined by friction welding. *Mater Des* 28(7):2244–2250
11. Nicholas ED (2003) Friction processing technologies. *Weld World* 47(11):2–9
12. Kimura M, Kusaka M, Kaizu K, Nakata K, Nagatsuka K (2016) Friction welding technique and joint properties of thin-walled pipe friction-welded joint between type 6063 aluminum alloy and AISI 304 austenitic stainless steel. *Int J Adv Manuf Technol* 82(1):489–499
13. Maalekian M (2007) Friction welding – critical assessment of literature. *Sci Technol Weld Join* 12(8):738–759
14. Luo J, Ye YH, Xu JJ, Luo JY, Chen SM, Wang XC, Liu KW (2009) A new mixed-integrated approach to control welded flashes forming process of damping-tube-gland in continuous drive friction welding. *Mater Des* 30(2):353–358
15. Sahin M (2009) Characterization of properties in plastically deformed austenitic-stainless steels joined by friction welding. *Mater Des* 30(1):135–144
16. Yilmaz M, Çöl M, Acet M (2003) Interface properties of aluminum/steel friction-welded components. *Mater Charact* 49(5):421–429
17. Kimura M, Ishii H, Kusaka M, Kaizu K, Fuji A (2009) Joining phenomena and joint strength of friction welded joint between aluminium–magnesium alloy (AA5052) and low carbon steel. *Sci Technol Weld Join* 14(7):655–661
18. James JA, Sudhish R (2016) Study on effect of interlayer in friction welding for dissimilar steels: SS 304 and AISI 1040. *Procedia Technol* 25:1191–1198
19. Wang T, Sidhar H, Mishra RS, Hovanski Y, Upadhyay P, Carlson B (2019) Effect of hook characteristics on the fracture behaviour of dissimilar friction stir welded aluminium alloy and mild steel sheets. *Sci Technol Weld Join* 24(2):178–184
20. Lee WB, Yeon YM, Kim DU, Jung SB (2003) Effect of friction welding parameters on mechanical and metallurgical properties of aluminium alloy 5052–A36 steel joint. *Mater Sci Technol* 19(6):773–778
21. Kimura M, Suzuki K, Kusaka M, Kaizu K (2017) Effect of friction welding condition on joining phenomena, tensile strength, and bend ductility of friction welded joint between pure aluminium and AISI 304 stainless steel. *J Manuf Process* 25:116–125
22. Kobayashi A, Machida M, Hukaya S, Suzuki M (2003) Friction welding characteristics of Al-Mg aluminum alloy (A5056) and carbon steel (S45C). *JSME Int J* 46(3):452–459
23. Fukumoto S, Tsubakino H, Okita K, Aritoshi M, Tomita T (1999) Friction welding process of 5052 aluminium alloy to 304 stainless steel. *Mater Sci Technol* 15(9):1080–1086
24. Kimura M, Kusaka M, Seo K, Fuji A (2005) Joining phenomena during friction stage of A7075-T6 aluminium alloy friction weld. *Sci Technol Weld Join* 10(3):378–383
25. Chen X, Li L, Zhou D (2016) Review on the formation and inhibition mechanism of Fe-Al intermetallic compound (in Chinese). *Int J Adv Manuf Technol* 30(7):125–132
26. Lee J-M, Kang S-B, Sato T, Tezuka H, Kamio A (2003) Evolution of iron aluminide in Al/Fe in situ composites fabricated by plasma synthesis method. *Mater Sci Eng A* 362(1):257–263
27. Huang Y, Wan L, Si X, Huang T, Meng X, Xie Y (2019) Achieving high-quality Al/steel joint with ultrastrong interface. *Metall Mater Trans A* 50(1):295–299
28. van der Rest C, Jacques PJ, Simar A (2014) On the joining of steel and aluminium by means of a new friction melt bonding process. *Scr Mater* 77:25–28
29. Reza-E-Rabby M, Ross K, Overman NR, Olszta MJ, McDonnell M, Whalen SA (2018) Joining thick section aluminum to steel with suppressed FeAl intermetallic formation via friction stir dovetailing. *Scr Mater* 148:63–67
30. Kato K, Tokisue H (2004) Dissimilar friction welding of aluminium alloys to other materials. *Weld Int* 18(11):861–867
31. Su H, Wu CS, Pittner A, Rethmeier M (2014) Thermal energy generation and distribution in friction stir welding of aluminum alloys. *Energy* 77:720–731
32. Wan L, Huang Y (2018) Friction stir welding of dissimilar aluminium alloys and steels: a review. *Int J Adv Manuf Technol* 99(5):1781–1811
33. Aghajani Derazkola H, Khodabakhshi F (2019) Intermetallic compounds (IMCs) formation during dissimilar friction-stir welding of AA5005 aluminum alloy to St-52 steel: numerical modeling and experimental study. *Int J Adv Manuf Technol* 100(9):2401–2422
34. Huang Y, Xie Y, Meng X, Lv Z, Cao J (2018) Numerical design of high depth-to-width ratio friction stir welding. *J Mater Process Technol* 252:233–241
35. Huang Y, Wan L, Meng X, Xie Y, Lv Z, Zhou L (2018) Probe shape design for eliminating the defects of friction stir lap welded dissimilar materials. *J Manuf Process* 35:420–427

Publisher's note Springer Nature remains neutral with regard to jurisdictional claims in published maps and institutional affiliations.